

# A dwarf galaxy remnant in Canis Major: the fossil of an in-plane accretion onto the Milky Way

N. F. Martin<sup>1</sup>, R. A. Ibata<sup>1</sup>, M. Bellazzini<sup>2</sup>, M. J. Irwin<sup>3</sup>, G. F. Lewis<sup>4</sup>, W. Dehnen<sup>5</sup>

<sup>1</sup> *Observatoire de Strasbourg, 11, rue de l'Université, F-67000, Strasbourg, France*

<sup>2</sup> *INAF - Osservatorio Astronomico di Bologna, Via Ranzani 1, 40127, Bologna, Italy*

<sup>3</sup> *Institute of Astronomy, Madingley Road, Cambridge, CB3 0HA, U.K.*

<sup>4</sup> *Institute of Astronomy, School of Physics, A29, University of Sydney, NSW 2006, Australia*

<sup>5</sup> *Department for Physics & Astronomy, University of Leicester, Leicester LE1 7RH, U.K.*

22 October 2018

## ABSTRACT

We present an analysis of the asymmetries in the population of Galactic M-giant stars present in the 2MASS All Sky catalogue. Several large-scale asymmetries are detected, the most significant of which is a strong elliptical-shaped stellar over-density, close to the Galactic plane at ( $\ell = 240^\circ, b = -8^\circ$ ), in the constellation of Canis Major. A small grouping of globular clusters (NGC 1851, NGC 1904, NGC 2298, and NGC 2808), coincident in position and radial velocity, surround this structure, as do a number of open clusters. The population of M-giant stars in this over-density is similar in number to that in the core of the Sagittarius dwarf galaxy. We argue that this object is the likely dwarf galaxy progenitor of the ring-like structure that has recently been found at the edge of the Galactic disk. A numerical study of the tidal disruption of an accreted dwarf galaxy is presented. The simulated debris fits well the extant position, distance and velocity information on the “Galactic Ring”, as well as that of the M-giant over-densities, suggesting that all these structures are the consequence of a single accretion event. The disrupted dwarf galaxy stream orbits close to the Galactic Plane, with a pericentre at approximately the Solar circle, an orbital eccentricity similar to that of stars in the Galactic thick disk, as well as a vertical scale height similar to that of the thick disk. This finding strongly suggests that the Canis Major dwarf galaxy is a building block of the Galactic thick disk, that the thick disk is continually growing, even up to the present time, and that thick disk globular clusters were accreted onto the Milky Way from dwarf galaxies in co-planar orbits.

**Key words:** Galaxy: structure – Galaxy: formation – galaxies: interactions

## 1 INTRODUCTION

It is now generally accepted that galaxies assembled by the hierarchical merging of dark matter halos (White, Rees 1978; White, Frenk 1991), with the accretion of luminous (dwarf) galaxies playing a significant, or probably even a major, role in the formation of the visible structures. In the Milky Way, this picture is dramatically illustrated by the existence of the Sagittarius dwarf spheroidal galaxy, which is in an advanced state of tidal disruption, and has populated the outer halo with M giant stars (Ibata et al. 2002), carbon stars (Ibata et al. 2001a) and globular clusters (Bellazzini, Ferraro & Ibata 2003).

The accretion of the Sagittarius galaxy is currently the only strong evidence that the Milky Way is absorbing satellite galaxies. However, the ring-like structure that has recently been discovered around the Galaxy could be the consequence of another such event. First discovered

as an over-density in blue stars of the Sloan Digital Sky Survey (Newberg et al. 2002), this “Ring” has since been probed using photometry from the INT Wide Field Camera (Ibata et al. 2003, hereafter I03), SDSS spectrometry and photometry (Yanny et al. 2003, hereafter Y03) and 2MASS M-giants (Rocha-Pinto et al. 2003). Surrounding the Galactic disk, its Galactocentric distance ranges from  $\sim 15$  kpc to  $\sim 20$  kpc in fields taken within  $30^\circ$  of the Galactic plane and for  $122^\circ < \ell < 227^\circ$ .

It has been proposed (I03 and Y03) that the structure could be the tidal stream stripped away by the Milky Way tides from a satellite galaxy that has an orbital plane close to the plane of the Galaxy. In light of this interpretation, it is interesting to reexamine the Abadi et al. (2002) simulation of the formation of a disk galaxy assembled hierarchically in a  $\Lambda$ CDM cosmology. They showed that the thin and thick disks of their simulated galaxy, which were similar to those

arXiv:astro-ph/0311010v1 1 Nov 2003

of the Milky Way, do not share the same origin. The simulated thick disk component was constructed mainly through accretions of satellites with an orbit close to the Galactic plane. These satellites are dense enough for their orbits to circularize before they are disrupted.

Helmi et al. (2003) also used this simulation to follow more closely the behavior of an in-plane accretion. They concluded that it naturally leads to the formation of a ring-like structure around the galaxy similar to the one found by Newberg et al. (2002), with two possible explanations. One possibility is that the ring is a tidal arc produced by stars stripped away from the parent satellite during a recent pericentric passage. This would produce an asymmetric structure above and below the disk, limited in Galactic longitude and with a significant velocity gradient in the Galactic longitude direction. Alternatively, it could be a shell-like structure, produced by ancient minor mergers, similar to the shells observed in elliptical galaxies. In this case, the ring would be rather symmetric and with no velocity gradient.

To discriminate between these competing scenarios, it is essential to analyze a large-scale, homogeneous data set. Until now, this was the main limitation, but with the release of the 2 Micron All Sky Survey, All Sky Release (2MASS ASR) catalogue we now have an invaluable tool to determine the characteristics of this Galactic “Ring”. Apart from covering all the sky, the 2MASS ASR contains precise near infrared photometry, so it is not much hampered by extinction in the low Galactic latitude regions with high dust-contamination where the “Ring” is primarily located.

We use this catalogue to probe the ring-like structure and determine its dimensions and characteristics on the celestial hemisphere opposed to the Galactic centre. In section 2, we discuss the data set we used for our study, presented in section 3. In section 4, we present the results of our search of clusters in the ring-like structure. Section 5 presents N-body simulations of the tidal disruption of the progenitor of the observed structures. Finally, in section 6, we discuss our results and the consequences on the origin of the “Ring”. Throughout this work, we assume that the Solar radius is  $R_{\odot} = 8$  kpc, that the LSR circular velocity is  $220 \text{ km s}^{-1}$ , and that the peculiar motion of the Sun is ( $U_0 = 10.00 \text{ km s}^{-1}$ ,  $V_0 = 5.25 \text{ km s}^{-1}$ ,  $W_0 = 7.17 \text{ km s}^{-1}$ ; Dehnen & Binney 1998b).

## 2 DATA

The low Galactic latitude regions that we study here are mainly hampered by two effects: by reddening due to the high concentration of dust in the Galactic plane and by the presence of numerous foreground disk stars. The 2MASS near infrared photometry has the ability to probe the highly obscured regions, but it cannot be directly used to remove the foreground disk stars. Therefore, in order to diminish the contamination of the closest disk stars, we cross-identified the 2MASS and the USNO-B1.0 catalogues in order to complement the 2MASS photometry with proper motion data. This was done for stars with  $|b| > 5^{\circ}$ .

In the present study we will work with two samples of stars: sample A is simply the 2MASS ASR point-source catalogue (with 2MASS flags `bl_flg = 111, cc_flg = 000, gal_contam = 0, mp_flg = 0`);

It will be used to search for the Galactic “Ring” population. Sample B is identical to sample A, except that we have removed all sources with significant ( $3\sigma$ ) proper motions. The contamination fraction of objects with proper motion corresponds to  $\sim 35\%$  of the 2MASS sources, but since they are irregularly distributed in a volume of a few kiloparsecs around the Sun this sample cannot be used to detect asymmetries. The proper motion discrimination is however very useful for plotting colour-magnitude diagrams: the disk dwarfs are particularly affected by this process and, since they tend to blend with red giant populations in CMDs, filtering them allows us to follow distant red giant branch (RGB) populations up to 2 magnitudes deeper. However, RGB stars beyond  $\sim 5$  kpc are not removed with this filter, judging from our tests in globular cluster fields (Martin 2003).

We de-redden the photometric data using the Schlegel, Finkbeiner & Davis (1998) algorithm which interpolates the  $E(B - V)$  value from the IRAS 100 micron emission all-sky maps. All the J, H,  $K_s$  magnitudes stated below are extinction-corrected. In order to use only precise photometry, we remove sources with  $K_s > 14.3$  (the 10-sigma limit of the 2MASS photometry) and with  $E(B - V) > 0.555$  (which corresponds to  $E(J - K_s) > 0.3$ ). This last limit mainly removes zones near the Galactic plane with  $|b| < 5^{\circ}$  from our samples. To make sure we can compare quantitatively the distribution of sources in both hemispheres, we divide the sky into  $0.1^{\circ} \times 0.1^{\circ}$  pixels (in Galactic coordinates) flagging as unusable each zone in which the extinction exceeds the chosen limit. However, to maintain North-South symmetry we also flag as unusable the symmetric pixel on the opposite side of the Galactic plane. We also limit our present samples to  $|b| < 40^{\circ}$ .

## 3 RESULTS

### 3.1 M-giant sample

From sample A, we first select a subsample of late M-giant stars using the same colour limits as Majewski et al. (2003):  $0.85 < J - K_s < 1.3$ ,  $J - H < 0.561(J - K_s) + 0.36$  and  $J - H > 0.561(J - K_s) + 0.22$ . We measure the distance of the Galactic M-giants using the RGB of the Sagittarius dwarf galaxy as a reference, as calibrated by Majewski et al. (2003):  $K_s = -8.650(J - K_s)_0 + 20.374$ . By assuming a distance modulus of  $m - M = 16.9$  for the stellar population at the core of the Sagittarius galaxy (Ibata et al. 1997), one can estimate the distance to other RGB populations. Figure 1 compares the 2MASS colour-magnitude diagrams (CMDs) of the Sagittarius dwarf with those of the Large Magellanic Cloud (LMC) and the globular cluster Omega Centauri; the corresponding distance calibrations are also displayed. The relatively poor fits for the LMC and Omega Cen, are probably due to differences in age and metallicity between these objects and the Sgr galaxy. Using the Sgr RGB calibration to measure the distances of the LMC and Omega Cen would incur a  $\sim 30\%$  systematic error, with these distances being underestimated. This systematic uncertainty will cloud all of the distances derived below for the Galactic M-giant population.

A comparison between the northern and southern hemispheres of the distribution of source distances, estimated

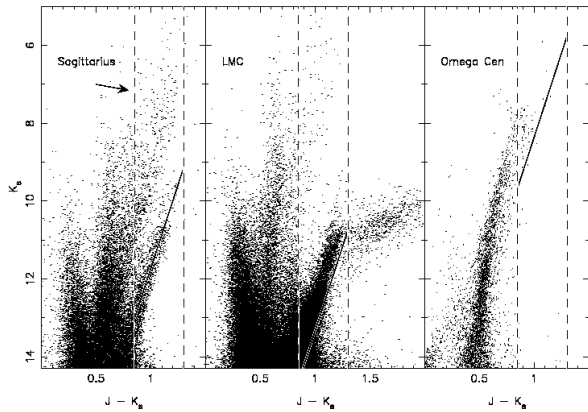


**Figure 1.** Comparison of colour-magnitude diagrams of our M-giant distance calibrator, the Sagittarius dwarf galaxy (left-hand panel), with the LMC (middle panel) and Omega Centauri (right-hand panel). The proper-motion cleaned catalogue (sample B) is used here. The Sgr CMD is derived from a  $1^\circ$  circle, centred on the core of the galaxy, the LMC CMD comes from an annulus between  $5^\circ$  and  $6^\circ$ , while the Omega Cen CMD is from data within  $20'$  of the core of the cluster. The  $J - K_s, K_s$  colour-magnitude selection window is shown between the dashed vertical lines (though note the additional selection in  $J - H$  colour is not displayed here). The arrow shows the reddening vector, with a length corresponding to the chosen reddening limit of  $E(B - V) < 0.555$ . In the left-hand panel, the solid line shows the Majewski et al. (2003) RGB calibration for the Sgr dwarf ( $m - M = 16.9$ ; Ibata et al. 1997). The parallel sequence approximately two magnitudes brighter than the Sgr RGB is the RGB of the bulge. The solid line in the middle and right-hand panels show the corresponding ridge line assuming a distance modulus of 18.515 for the LMC (Clementini et al. 2003) and 13.53 for Omega Cen (Harris 1996). Using the Sgr fiducial to determine the distance to the LMC or Omega Cen would lead to a  $\sim 30\%$  underestimate of their distances. The substantial population red-ward of  $J - K_s = 1.3$  in the LMC are AGB carbon stars, which highlights the need for the upper  $J - K_s$  colour limit.

from sample A, using the Sgr RGB fiducial described above, shows two striking asymmetries, one in each hemisphere (see Figure 2). The southern over-density, located between  $220^\circ < \ell < 260^\circ$  is the most significant (detected with  $S/N = 30$ ). It ranges from 10.0 kpc to 15.8 kpc from the Galactic centre and is centred at  $\sim 12.6$  kpc. The northern over-density ranging from  $\ell = 140^\circ$  to  $\ell = 220^\circ$  is further away, between 15.8 kpc and 20.9 kpc, with its maximum between 16.6 kpc and 19.0 kpc (this peak is detected at  $S/N = 13$ ). In both cases there are approximately twice as many stars in the over-density than in the other hemisphere.

To examine the structures creating these two over-densities, the data in sample A was binned in Galactic coordinates, as presented in Figure 3. In those pixels where more than 50% of the area is below the extinction limit, we have corrected the counts for the area incompleteness; otherwise, the pixel values are set to zero. We impose North-South symmetry to be able to compare the counts between the hemispheres. In the southern hemisphere, for the  $15.2 < (m - M)_{GC} < 15.7$  range, an object is centred at

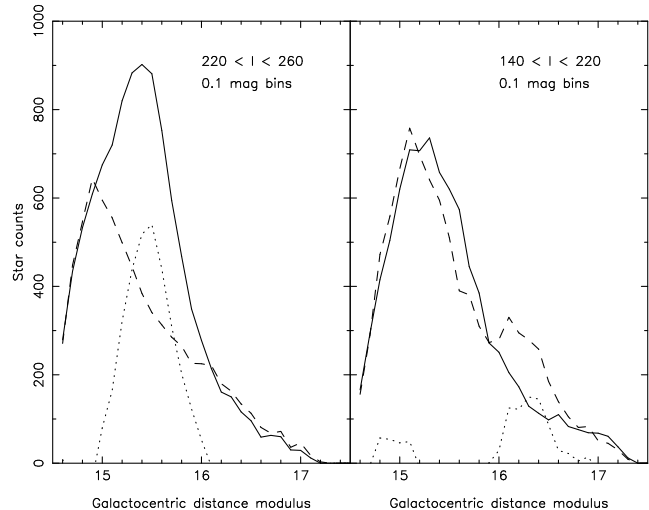


**Figure 2.** The Galactocentric distance modulus  $(m - M)_{GC}$  distribution for M-giant stars in sample A with  $|b| < 40^\circ$ ,  $E(B - V) < 0.555$  and for different ranges in  $\ell$ . Note that in this, and all subsequent figures, those regions removed by the extinction cut have their corresponding symmetric region about the Galactic plane removed as well. The star distribution in the southern hemisphere (full line) is compared to the northern hemisphere distribution (dashed line); the difference between these distributions is also plotted (dotted line). The  $220^\circ < \ell < 260^\circ$  region (left panel) shows an over-density in the southern hemisphere, ranging over  $15.0 < (m - M)_{GC} < 16.0$  with a maximum at  $(m - M)_{GC} = 15.5$  (the signal to noise ratio of this peak is  $S/N = 30$ ). The  $140^\circ < \ell < 220^\circ$  region (right panel) shows an over-density in the northern hemisphere, ranging over  $16.0 < (m - M)_{GC} < 16.6$  with a maximum between  $(m - M)_{GC} = 16.1$  and  $(m - M)_{GC} = 16.4$  (this peak has  $S/N = 13$ ).

$\ell \sim 240^\circ$  and  $b \sim -8^\circ$ , in the direction of the Canis Major constellation. It is very dense at its core — with up to eight times the number of stars compared to the symmetric zone in the northern hemisphere — and it seems to be approximately elliptical. These structures are more clearly seen in the difference image displayed in Figure 4, where we have subtracted the star-counts from the opposite hemisphere. The Canis Major over-density is striking, as is the wide arc-like structure in the northern hemisphere. The location of these features is made clearer with schematic overlays in Figure 5.

To measure the dimensions of the Canis Major object, we examine the profiles in the latitude and Heliocentric distance directions (Figure 6). Analysis of the vertical distribution of the population is hampered by the lack of non-dust-contaminated regions for  $|b| < 7^\circ$ . This puts a high degree of uncertainty on the profile fits since the population could correspond to a Gaussian distribution centred at  $b = -6.3^\circ \pm 1.0^\circ$  with a FWHM vertical height of  $1.6 \pm 0.2$  kpc, or alternatively, an exponential distribution with a  $0.73 \pm 0.05$  kpc scale height. It is interesting to note that this scale height derived for the Canis Major structure at  $\ell = 240^\circ$  is statistically identical to that obtained by I03 for the Galactic Ring, in a field at  $\ell = 123^\circ$ . This lends some support to the possibility that the structures are related. The Heliocentric distribution of the object can be fit

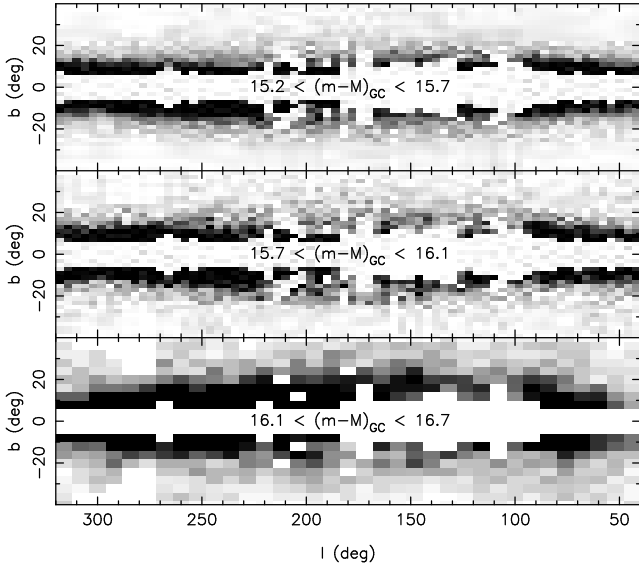


**Figure 3.** The distribution of M-giant stars (from sample A) for different ranges in Galactocentric distance modulus  $(m - M)_{GC}$ . (We choose to display these distributions in Galactocentric coordinates because the over-densities are more peaked than in Heliocentric coordinates, whereas the use of the distance modulus makes it easier to visualize the effects of extinction and population differences). In the upper two panels a pixel corresponds to a  $4^\circ \times 2^\circ$  rectangle, while in the bottom panel a pixel covers  $8^\circ \times 4^\circ$ ; the scale colour is different for each panel to emphasize the structures. The circular hole at  $l \sim 280^\circ$  and  $b \sim -35^\circ$  comes from the removal of the Large Magellanic Cloud; due to the symmetry imposed on the map, this hole is reflected in the North as well. The top panel contains the sources of our sample with  $15.2 < (m - M)_{GC} < 15.7$ . The most significant over-density in this distance range is created by a dense object at  $220^\circ \lesssim l \lesssim 260^\circ$  and  $b \gtrsim -20^\circ$ , towards Canis Major. The middle panel shows the distribution of sources with  $15.7 < (m - M)_{GC} < 16.1$ , while the bottom panel shows  $16.1 < (m - M)_{GC} < 16.7$ . In the top, middle and bottom panels, a black pixel corresponds to 40, 16 and 16 counts, respectively.

by a Gaussian centred at  $D_\odot = 7.1 \pm 0.1$  kpc with FWHM of  $4.2 \pm 0.3$  kpc. While the centre of the distribution can be measured reliably, its FWHM should be taken with caution since the distribution is skewed to large distances. This could be due to the angle of observation of the structure if it is elongated in a direction that is not perpendicular to the line of sight. The precise extent of this object along the longitude axis is harder to compute because the observations are hampered by high extinction regions and by the rapid increase in the number of disk stars at low latitude.

The Northern Arc over-density is visible for  $16.1 < (m - M)_{GC} < 16.7$  (bottom panel of Figures 3 and 4). It begins near the Galactic plane at  $l \sim 230^\circ$  and then arcs up to  $l \sim 140^\circ$  and  $b \sim +30^\circ$ . The best region to compute its vertical height is between  $140^\circ < l < 180^\circ$  because it is further away from the Galactic disk than elsewhere. We find there that the Northern Arc has a Gaussian profile (see Figure 7), centred on  $19.9^\circ \pm 1.0^\circ$  and with a  $2.2 \pm 0.4$  kpc vertical width. However, high extinction regions could be responsible for the decrease of star counts under  $b \sim 15^\circ$  and the vertical width could be underestimated. The thickness of the structure was also

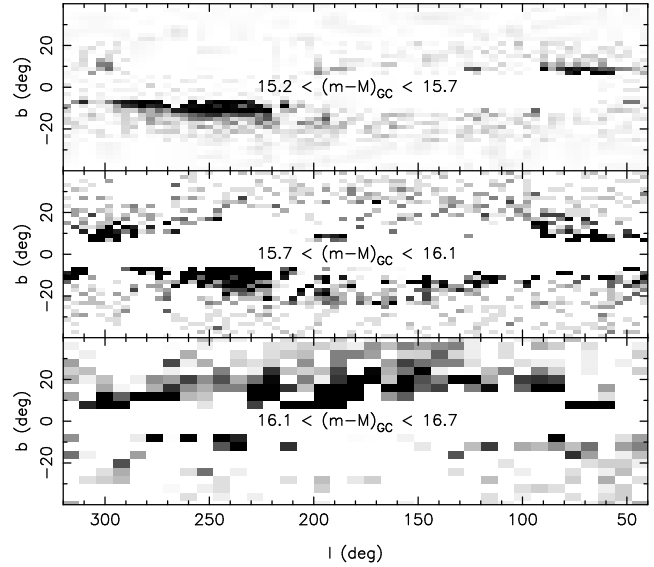


**Figure 4.** As Figure 3, but showing the difference in M-giant starcounts between the two hemispheres. The Canis Major over-density at ( $l \sim 240^\circ, b \sim -10^\circ$ ) is clearly visible on the upper two panels. The middle panel also shows a fainter population arcing over the sky between  $110^\circ \lesssim l \lesssim 210^\circ$  in the southern hemisphere. Another huge arc-like structure is present in the northern hemisphere in the bottom panel ranging from  $l \sim 140^\circ$  to  $l \sim 220^\circ$ . In the top, middle and bottom panels, a black pixel corresponds to 40, 8 and 8 counts, respectively.

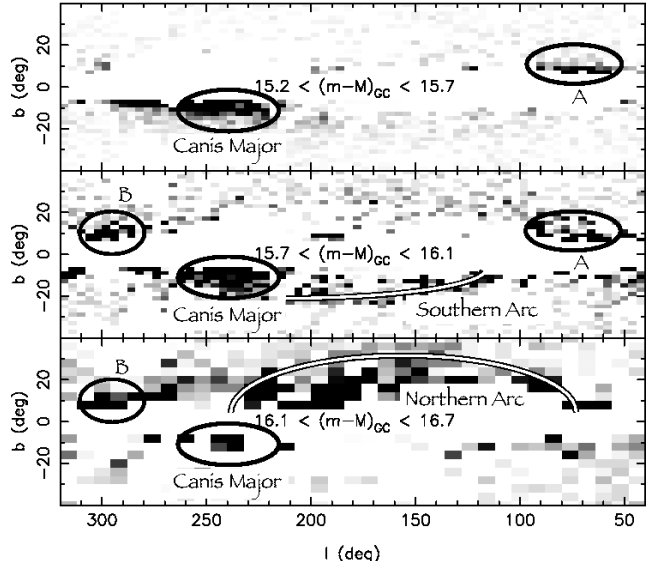


**Figure 5.** As Figure 4, with an overlay of the main asymmetries in the Galactic M-giant distribution detected in Figures 3 and 4. The strongest of these is the Canis Major over-density, followed by the Northern Arc. A fainter Southern Arc is also visible, as are two structures at  $l = 70^\circ$ , and  $l = 300^\circ$ , which we label structures A and B respectively.

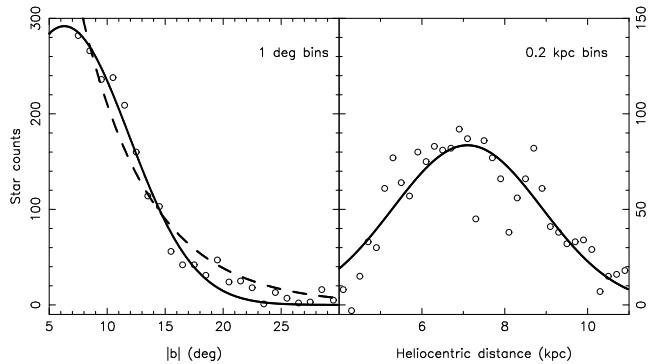


**Figure 6.** Vertical and radial profiles of the Canis Major object, derived from sample A. The northern hemisphere is used as a reference and its star counts are subtracted from those of the southern hemisphere. The left-hand panel shows the latitude distribution of stars with  $15.2 < (m - M)_{GC} < 15.7$  and  $220^\circ < \ell < 260^\circ$ . The lack of data for  $|b| < 7^\circ$  puts a high degree of uncertainty on the fits, but the best Gaussian fit (full line) is centred on  $b = -6.3^\circ \pm 1.0^\circ$  with a FWHM of  $13.1^\circ \pm 1.3^\circ$ , corresponding to a latitude width of  $1.6 \pm 0.2$  kpc. We also calculated the best exponential fit of the population (dashed line): it has a scale height of  $0.73 \pm 0.05$  kpc. The right-hand panel shows the radial distribution of stars for the region of the centre of the object ( $230^\circ < \ell < 250^\circ$  and  $-12^\circ < b < -7^\circ$ ). The best Gaussian fit has been superposed on the star counts: it corresponds to a Gaussian centred on  $D_\odot = 7.1 \pm 1.3$  kpc, with a  $4.2 \pm 0.3$  kpc FWHM. We used the Heliocentric distance distribution here because our angle selection was made in Heliocentric coordinates, more suited for observations along these lines of sight.

computed, this time in the region where the over-density is most pronounced in the northern hemisphere, that is for  $140^\circ < \ell < 180^\circ$  and  $+10^\circ < b < +25^\circ$ . The right-hand panel of Figure 7 shows the best Gaussian fit for the radial profile of the structure: centred on  $D_{GC} = 18.1 \pm 0.1$  kpc, it has a FWHM line of sight thickness of  $2.2 \pm 0.3$  kpc. This structure is almost certainly due to the M-giants present in the “Galactic Ring” of I03 and Y03. Even with the rather noisy values derived here, the Gaussian vertical FWHM falls in the range of the Y03 and I03 exponential scale height measurements (respectively  $< 4$  kpc and  $\sim 2$  kpc).

A second southern over-density, the “Southern Arc” in Figure 5, ranges over  $110^\circ < \ell < 210^\circ$  and  $12.0$  kpc  $< D_{GC} < 15.1$  kpc (i.e.  $15.4 < (m - M)_{GC} < 15.9$ ). This structure is detected at  $S/N = 8$ . It is possible that its vertical distribution has a similar Gaussian profile to that of the Northern Arc, but the large highly dust-contaminated region near the disk hampers the interpretation of the observations. This feature may correspond to the southern hemisphere population reported by Y03 in the longitude range  $180^\circ < \ell < 227^\circ$  and at a distance of  $R_{GC} = 20 \pm 2$  kpc. The 30% systematic distance error mentioned earlier may be responsible for the difference in these two distance estimates.

The two main over-densities can be followed around half of the Milky Way. To diminish the projection problems that appear when observing in the quadrant towards the Galactic centre (i.e. for  $\ell > 270^\circ$  and  $\ell < 90^\circ$ ), we switched to the Galactocentric cylindrical coordinates  $(R, \Phi, z)$ . We also limited our sample to  $|b| < 30^\circ$  since the sources are further away from the Sun. The left panel of Figure 8 shows the Galactocentric distance modulus distribution of stars

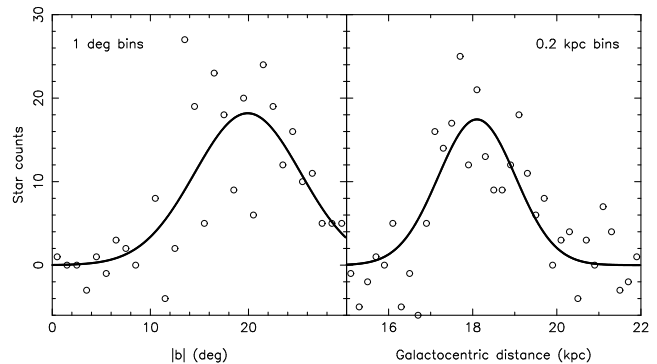


**Figure 7.** Profiles of the Northern Arc structure. The southern hemisphere is used as a reference and its star counts are subtracted from those of the northern hemisphere. The left-hand panel shows the latitude profile of the structure for  $140^\circ < \ell < 180^\circ$  and  $16.1 < (m - M)_{GC} < 16.7$ , and the best Gaussian fit of the star counts. The distribution has a mean value of  $19.9^\circ \pm 1.0^\circ$  and a FWHM of  $12.7^\circ \pm 2.3^\circ$ . At the Heliocentric distance of the object ( $\sim 10$  kpc), it corresponds to a vertical width of  $2.2 \pm 0.4$  kpc. The right-hand panel shows the radial profile of the structure for  $140^\circ < \ell < 180^\circ$  and  $+10^\circ < b < +25^\circ$ . The distribution is centred on  $D_{GC} = 18.1 \pm 0.1$  kpc with a  $2.2 \pm 0.3$  kpc thickness. Since here the observations are in the direction of the anticentre, we were able to use Galactocentric distances.

for  $230^\circ < \Phi < 270^\circ$  where the prolongation of the Canis Major over-density is visible despite the higher number of disk stars. It ranges up to  $D_{GC} \sim 14.5$  kpc from at least  $D_{GC} = 5$  kpc but the presence of the bulge prevents the determination of a precise lower limit. The high radial extent of the over-density is certainly due to the angle of observation. Indeed, it is possible that the structure is, at least partially, not observed perpendicularly but rather tangentially. This would also explain its broad profile and seems to be confirmed when taking smaller ranges of  $\Phi$ . The right-hand panel corresponds to  $90^\circ < \Phi < 130^\circ$  and shows the prolongation of the Northern Arc. It ranges over  $7.2$  kpc  $\lesssim D_{GC} \lesssim 16.6$  kpc which is nearer from the Galactic centre than it was in the direction of the anticentre. It is surprising to find that it is also denser. This could also be due to the angle of observation: if here too we are partially observing the structure tangentially, the star counts will be summed up along the line of sight.

To summarize, we were able to detect two substantial over-densities of M-giants, the Canis Major over-density and the Northern Arc, which together surround half of the Milky Way, at varying Galactocentric radius. This population can be as close as 5 kpc from the Galactic centre for  $\Phi = 90^\circ$  and 20 kpc away in the direction of the anticentre. We also find it probable that it passes from the northern to the southern hemisphere at around  $\ell = 230^\circ$ .

### 3.2 Colour-Magnitude Diagrams

We now examine the stellar populations of the stars in the structure, using the near infrared 2MASS photometry. As can be discerned in Figure 9, the  $(J - K_s, K_s)$  CMD of a  $5^\circ \times 2^\circ$  region at the centre of the Canis Major object shows two striking features: a red-giant branch population which does not appear on the reference CMD on the other

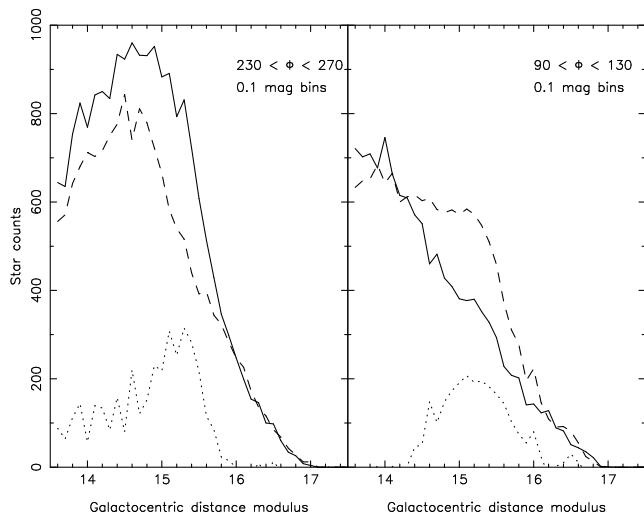


**Figure 8.** The Galactocentric distance modulus  $(m - M)_{GC}$  distribution for M-giant stars with  $|b| < 30^\circ$ ,  $E(B - V) < 0.555$  and for different ranges of the Galactocentric cylindrical coordinate  $\Phi$ . The star distribution in the southern hemisphere (full line) is compared to the northern hemisphere distribution (dashed line); the over-densities are also plotted (dotted line). The  $230^\circ < \Phi < 270^\circ$  region (left panel), which corresponds to  $\ell \gtrsim 270^\circ$ , shows the prolongation of the Canis Major over-density. With a Galactocentric distance modulus of  $(m - M)_{GC} < 15.8$ , it is closer to the Galactic centre than the over-density we presented on Figure 2; the  $(m - M)_{GC} = 13.5$  lower limit is due to the presence of the bulge. The over-density has a maximum star count of  $\sim 300$  (per interval of 0.1 in distance modulus) at  $(m - M)_{GC} = 15.1$  and slowly decreases with decreasing distance from the Galactic centre. The  $90^\circ < \Phi < 130^\circ$  region (right panel), which corresponds to  $\ell \lesssim 90^\circ$ , shows the feature labeled as structure “A” in Figure 5, which may be the prolongation of the Northern Arc. It is also nearer, ranging over  $14.3 < (m - M)_{GC} < 16.1$  centred around  $(m - M)_{GC} = 15.1$ , with a profile that is approximately symmetric.

side of the Galactic plane and a high number of stars for  $0.55 \lesssim J - K_s \lesssim 0.65$  and  $12 \lesssim K_s \lesssim 13.5$ . For comparison, we superimpose on Figure 9 the line of the fiducial RGB sequence of the Sgr dwarf, adjusted to 7.1 kpc, the distance of the Canis Major structure determined from the analysis of Figure 6. Inspection of the subtracted Hess-diagram shown in the right-hand panel of Figure 9 reveals that the population in this central field  $5^\circ \times 2^\circ$  is slightly ( $\sim 1.5$  kpc) more distant, than estimated above. An alternative explanation could be that there is a stellar population gradient towards the centre of the structure.

This excess RGB population does not appear to be spatially separated from the Galactic disk, that is, we do not detect a magnitude gap separating this population and the disk red giants in the data presented in the left-hand panel of Figure 9. The structure therefore lies within, or at the edge, of the Galactic disk. The other feature that is present at the bottom of this red giant branch (at  $0.55 < J - K_s < 0.65$ ,  $K_s \sim 12.5$ ) is the corresponding red clump of the stellar population. An additional blue plume at  $J - K_s < 0.5$  is seen in the subtracted Hess diagram; this feature could be an intermediate-age main-sequence population of the Canis Major galaxy, although it could possibly also be an artifact

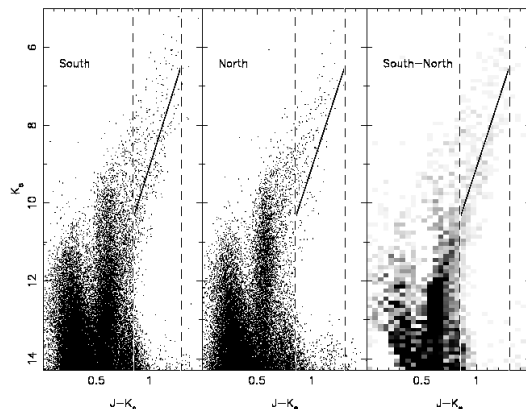


**Figure 9.** Near infrared colour-magnitude diagrams (from the proper-motion cleaned sample B) of the centre of the Canis Major object ( $239^\circ < \ell < 244^\circ$  and  $-10^\circ < b < -8^\circ$ ) and its symmetric region in the northern hemisphere ( $239^\circ < \ell < 244^\circ$  and  $8^\circ < b < 10^\circ$ ). The Canis Major object CMD shows two features which are not in the reference CMD, and that are clearly seen in the subtracted Hess diagram shown on the right-hand panel (a black pixel corresponds to a count of 25 stars). A red-giant branch is present from  $(J - K_s \sim 0.7, K_s \sim 12)$  to  $(J - K_s \sim 1.2, K_s \sim 8)$ , while the dense feature at  $(0.55 < J - K_s < 0.65, K_s \sim 12.5)$  is the red clump. As in Figure 1, the dashed lines show part of the colour-magnitude selection region. The solid lines show the RGB fiducial of the Sgr dwarf galaxy (left-hand panel of Figure 1), adjusted to a distance of 7.1 kpc (the distance to the structure determined from the analysis presented in Figure 6).

of the subtraction. A deeper optical wide-field survey of the region may help resolve this issue.

The colour-magnitude diagram of the Northern Arc reveals a sparse red giant branch, consistent with a Galactocentric distance of  $\sim 18.1$  kpc, as we show in the left-hand panel of Figure 10. It appears that there is a small gap between the RGB of this population, and the disk RGB stars, indicating that the structure is separated from the disk at its most distant point. The middle panel of Figure 10 shows a comparison region below the Galactic plane; here, we may also have detected a similar RGB population, though the signal is very weak. This feature may correspond to the “Southern Arc” structure highlighted in Figure 5.

We also searched for the RGB population of the structure in small low extinction windows at very low latitude. However, the low number of the M-giants of interest compared to the high number of stars in the disk prevents any further conclusion on the connection between the Northern Arc and the Canis Major over-densities. The RGB populations for  $230^\circ < \Phi < 270^\circ$  and  $90^\circ < \Phi < 130^\circ$  also have low contrast because the structures are mixed with the disk and the higher number of disk stars weakens the signal due to the over-densities.

### 3.3 Extinction

Could these inferred over-densities simply be due to errors in the Schlegel, Finkbeiner & Davis (1998) extinction maps? The colour of the vertical CMD feature of disk dwarfs in the

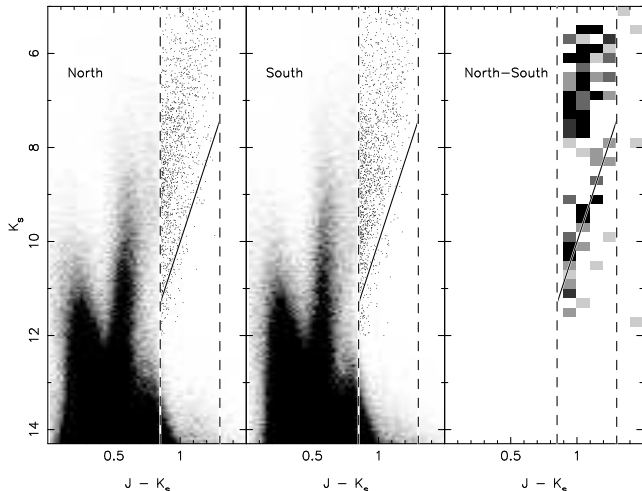


**Figure 10.** The left-hand panel shows the near infrared colour-magnitude diagram (from the proper-motion cleaned sample B) of a  $15^\circ \times 15^\circ$  region in the Northern Arc over-density ( $140^\circ < \ell < 155^\circ$  and  $10^\circ < b < 25^\circ$ ). Since the Northern Arc is fainter than the Canis Major structure, it is necessary to gather sources over a wider area to obtain sufficient signal to render the excess M-giant population visible. For clarity, we use a Hess diagram, except in the colour-magnitude region  $J - K_s > 0.85$ ,  $K_s < 12.0$ . The solid line shows the position of the fiducial Sgr dwarf RGB, shifted to an equivalent Galactocentric distance of 18.1 kpc, as indicated by the analysis presented in Figure 7. A population of stars is clumped around this line, indicating the presence of an RGB at this distance. A gap between the RGB of the Northern Arc over-density and the RGBs of the disk can also be perceived, indicating that the structure is separated from the disk in this direction. The middle panel shows the Hess diagram and CMD of the symmetric region about the Galactic Plane ( $140^\circ < \ell < 155^\circ$  and  $-25^\circ < b < -10^\circ$ ). A hint of the same RGB is also present, though the population is much less numerous; it probably corresponds to the “Southern Arc” identified in Figure 5. Due to the low contrast of the population over the numerous foreground, it proved hard to construct a clear subtracted Hess diagram. Our best attempt, shown on the right-hand panel, reveals the presence of an RGB-like population beneath the solid line; here a black pixel corresponds to 5 stars. The red clump population, however, is lost in the noise of the local disk red dwarf sequence.

extinction-corrected samples is almost identical (to within  $\sim 0.1$  magnitudes) North and South of the Galactic plane. This is demonstrated in Figure 9, where the sequence of disk dwarfs is seen both on the left-hand panel at  $J - K_s \sim 0.6$  in the over-density at ( $\ell = 242^\circ, b = -9^\circ$ ), and at the same colour in the symmetric field about the Galactic Plane ( $\ell = 242^\circ, b = 9^\circ$ ). Additionally, this sequence is detected in low extinction regions at the same  $J - K_s$  colour, giving us further confidence that the Schlegel, Finkbeiner & Davis (1998) extinction maps are not significantly in error along these sight-lines.

For the RGB-like population present on the subtracted Hess diagram on the right-hand panel in Figure 9 to be caused by extinction errors, would require a contaminating population that runs parallel to that RGB population (but both bluer and brighter). The only available population that has this property is the RGB of the Galactic disk. However, inspection of Figures 2 and 8 shows that the distribution of M-giants on opposite sides of the Galactic Plane match well

at the lower distance limits and at the upper distance limits of those diagrams. It is at intermediate distances that a discrepancy is detected. Extinction errors can only rearrange the distance distributions, they cannot cause an apparent overabundance of stars all along the RGB. For these reasons it is unlikely that the detected over-densities are extinction artifacts.

### 3.4 Mass of the Canis Major structure

To estimate the mass of the Canis Major object, we compare the number of detected M-giants to those observed in the Sagittarius dwarf galaxy. For Canis Major, we subtract the northern hemisphere sample A data from the southern hemisphere and sum under the profiles shown in Figure 6. Within a  $10^\circ$  radius region (but which misses  $\sim 40\%$  of the area due to the  $|b| < 5^\circ$  cutoff and due to the  $E(B - V) < 0.555$  reddening limit) we detect 2300 M-giants. The same measurement around the core of the Sagittarius dwarf galaxy gives an almost identical number of 2200 M-giants. With the caveat that the stellar populations are not the same, this suggests that the Canis Major object has a similar total luminosity to the core of the Sagittarius dwarf galaxy, which has been measured to be  $M_V = -13.27$  (Majewski et al. 2003). If we further assume that the mass to light ratio of the two galaxies is similar, we conclude that the Canis Major object has an almost identical mass to that of the core of the Sagittarius dwarf. The mass of the latter is a matter of some debate (Ibata et al. 1997; Ibata & Lewis 1998; Helmi & White 2001; Gómez-Flechoso, Fux & Martinet 1999), but a range between  $10^8 M_\odot$  to  $10^9 M_\odot$  seems plausible, with the upper bound being the likely pre-disruption mass of that galaxy.

## 4 A CLUSTERING OF GLOBULAR CLUSTERS

While searching for structures in the Galactic globular cluster system that could be connected with the stream of the Sagittarius galaxy (Bellazzini, Ferraro & Ibata 2003; Bellazzini et al. 2003b), we noted an interesting group of clusters that are not related with Sgr and that are remarkably confined in phase space (Bellazzini et al. 2003c). These four clusters, NGC 1851, NGC 1904, NGC 2298 and NGC 2808, are quite close to one another in space, indeed, they may be enclosed in a sphere with radius  $R \simeq 6$  kpc centred at Galactic Cartesian coordinates  $(X, Y, Z) = (-11.5, -8.9, -4.5)$  kpc. Among the outer halo globular clusters (those with  $R_{GC} > 10$  kpc, see Bellazzini, Ferraro & Ibata 2003) there is only one other group of globulars that shows similar clustering properties, the clusters associated with the main body of the Sgr dSph galaxy (M 54, Ter 7, Ter 8, and Arp 2). In Figure 11 the spatial distributions of the two groups are compared in two different projections of Cartesian Galactocentric coordinates: NGC 1851, NGC 1904, NGC 2298 and NGC 2808 are as close one to another as the Sgr globulars. It is interesting to recall that the similar proximity of the four Sgr cluster was not noted until the discovery of their parent galaxy (Bellazzini et al. 2003c).

If we consider the radial velocities, the present Sgr globular cluster system appears much more compact

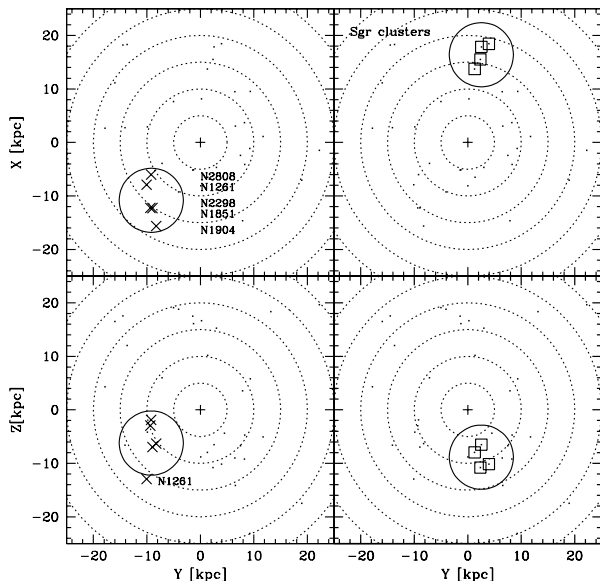


**Figure 11.** Comparison of the clustering properties in space of the group of globulars NGC 1851, NGC 1904, NGC 2298, NGC 2808, NGC 1261 (left panels) and of the globular clusters associated with the main body of the Sgr galaxy (right panels; M 54, Ter 7, Ter 8, and Arp 2). The clusters are plotted in Cartesian Galactocentric projections (upper panels: YX; lower panels: YZ). In this coordinate system the Galactic Centre is at  $(X, Y, Z) = (0, 0, 0)$  kpc and the Sun is at  $(X, Y, Z) = (-8, 0, 0)$  kpc. The small cross indicates the Galactic Centre and the dotted circles have Galactocentric radius from  $R = 5$  kpc to  $R = 30$  kpc, in steps of 5 kpc. Both groups are enclosed in a (continuous) circle having radius  $r = 6$  kpc.

( $\sigma_{V_{LSR}} = 21.5 \text{ km s}^{-1}$ ) than the considered group ( $\sigma_{V_{LSR}} = 95.3 \text{ km s}^{-1}$ ). However the data presented in Figure 12 show that the LSR-corrected radial velocity of the group members correlates well with Galactic longitude. Moreover, their Galactocentric distance also correlates with Galactic longitude. These facts are strongly suggestive of a coherent motion along a common orbit.

After the discovery of this remarkable phase space grouping of globular clusters we noted that their positions are virtually coincident with the Canis Major structure discussed in this paper. The strong analogy with the Sgr case brings us to the conclusion that the two structures are associated and that NGC 1851, NGC 1904, NGC 2298 and NGC 2808 are likely the local remnant of the globular cluster system of the galaxy that was the progenitor of the Canis Major object and the Northern Arc.

These clusters also show some interesting similarities in their intrinsic properties. For instance, their metallicity is enclosed in the relatively limited range  $-1.03 \leq [\text{Fe}/\text{H}] \leq -1.71$ , all of them show an extended blue Horizontal Branch in their colour-magnitude diagrams, and NGC 1851 and NGC 2808 are the only two halo clusters showing simultaneously a well populated red clump and a blue tail in their HB morphology (see Harris 1996; Bedin et al. 2000; Bellazzini et al. 2001, and references therein).

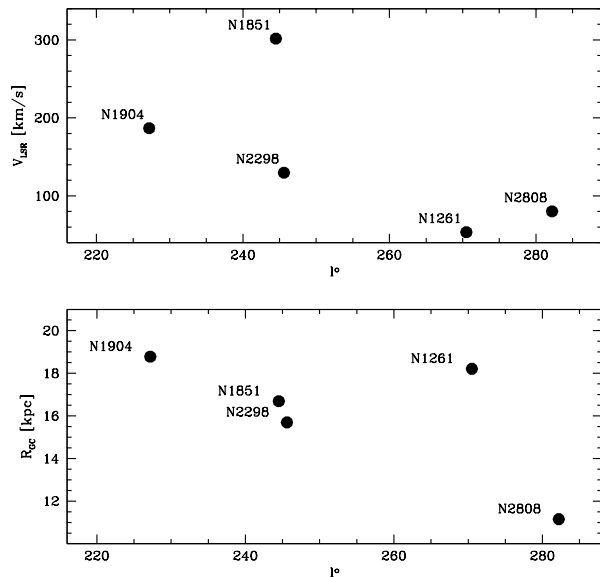


**Figure 12.** The upper panel shows the correlation between Galactic longitude and the radial velocity (corrected for the motion of the Local Standard of Rest) for the clusters associated with the Canis Major object. The lower panel presents the correlation between Galactic longitude and Galactocentric distance.

There are other globular clusters that may be related to the Canis Major structure. NGC 1261 is also nearby in space to the above described group but its velocity does not fit well with the velocity gradients shown in Figure 12. We will return to this issue in Section 5 below.

It is also interesting to study the distribution of open clusters in light of the discovery of the Canis Major object. Figure 13 shows the open clusters in the WEBDA database (Mermilliod 1995)<sup>1</sup> with  $D_{\odot} > 6$  kpc; a puzzling asymmetry is evident with absolutely no clusters for the  $\ell < 180^{\circ}$  part of the Milky Way. Caveats may include strong uncertainties in distance and/or age since the directions are often obscured and the cluster population is small. Moreover, the presence of the Outer Arm of the Galaxy could provide a stronger background in the  $0^{\circ} < \ell < 180^{\circ}$  quadrant against which it could be more difficult to identify clusters. On the other hand, part of the  $180^{\circ} < \ell < 270^{\circ}$  quadrant is behind the Perseus Arm which is much closer to the Sun: Therefore the considered region suffers from a less severe contamination and the identification of remote clusters is easier.

With these caveats in mind, it is still possible that part of these remote open clusters belong to the Canis Major galaxy. In particular Dol 25 ( $\ell = 211.9^{\circ}, b = -1.29^{\circ}$ ) and H 18 ( $\ell = 243.1^{\circ}, b = 0.44^{\circ}$ ) which are both young ( $\log(\text{age}) < 8.5$ ) and with a Heliocentric distance that corresponds to the Canis Major object could be the consequence of a strong perturbation of the disk by the accreted dwarf Galaxy and the resulting enhanced star-formation activity

<sup>1</sup> The WEBDA database, developed and maintained by J.-C. Mermilliod, can be found on <http://obswww.unige.ch/webda/webda.html>



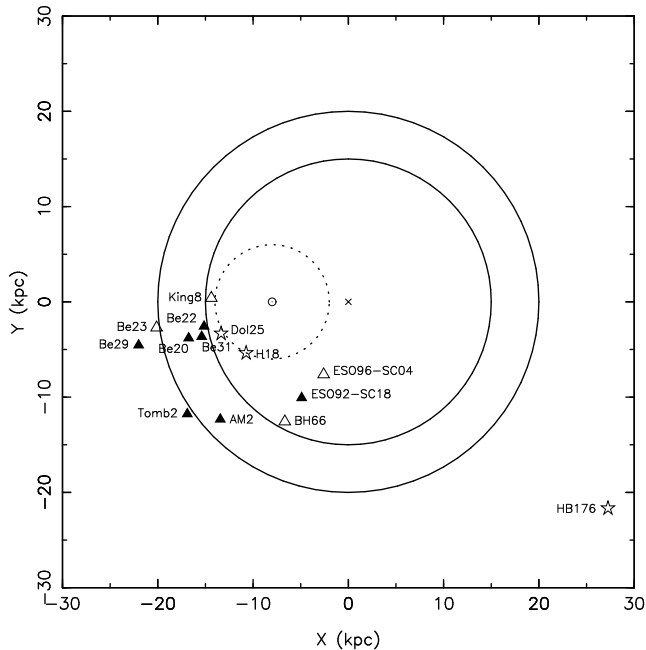


**Figure 13.** Distribution of open clusters with  $D_{\odot} > 6$  kpc. The Galactic centre has been marked (cross) as well as the Sun (dotted circle). The full line circles correspond to a distance of 15 kpc and 20 kpc from the Galactic centre; the dotted circle corresponds to the  $D_{\odot} = 6$  kpc limit. The symbols correspond to the estimated age of the open clusters:  $\log(\text{age}) < 8.5$  (stars),  $8.5 < \log(\text{age}) < 9.0$  (empty triangles) and  $\log(\text{age}) > 9.0$  (filled triangles). All the open clusters have  $|b| < 18^{\circ}$ .

in the disk. We also note that the position of the old open cluster AM2 (previously classified as a globular) nearly coincides with that of the central peak of the Canis Major structure, within the (large) distance uncertainties. Unfortunately the lack of any radial velocity estimate for this cluster prevents any definite conclusion about its possible physical association with the newly discovered object.

## 5 N-BODY SIMULATION

We undertook a series of N-body experiments in an attempt to determine whether a single accretion of a dwarf galaxy could be responsible for the detected over-densities and the correlations seen among globular and open clusters. In this first study, we concentrate on constructing a simple model to guide interpretation of the observations, and will defer a more detailed analysis to a subsequent contribution.

For our simulations, we take a static Milky Way potential, which is not perturbed by the passage of the accreted dwarf galaxy. The potential model 2b of Dehnen & Binney (1998a) is adopted, but with the halo component modeled by a spherical NFW halo. Taking a static potential is unrealistic, of course, but it saves a great deal of computation time, making the simulation tractable. The key effects that this approach leaves out are the back-reaction of the dwarf galaxy on the Galactic disk, and the back-reaction on the halo. The disk will likely become deformed (though note that the progenitor of the Galactic “Ring” has an angular momentum vector that is almost at right angles to that of the

Galactic warp, so it is unlikely to warp the disk strongly), and these deformations will in turn alter the trajectory of the accreted object. Since we do not include a live halo component, we neglect the back-reaction on the halo (formation of a wake), and the resulting dynamical friction on the dwarf galaxy.

A useful working picture is that the dwarf galaxy began its life as a typical dark matter-dominated dwarf satellite galaxy, far away in the Milky Way halo. The dark matter halo of the dwarf galaxy became progressively more and more disrupted as the orbit decayed. However, the central stellar component stayed largely intact during this initial phase. We start our simulation 2 Gyr ago, and assume that by this stage much of the dark matter has been removed from the system, leaving a much less massive dwarf galaxy that will not suffer significant dynamical friction. We therefore do not add dynamical friction in our simulation.

The simulations were performed with *falcON*, a fast and momentum-conserving tree code (Dehnen 2000, 2002). Gravity was softened with the kernel “P<sub>2</sub>”, with a softening length of 0.1 kpc. The minimum time-step was set to  $2^{-14} = 6.1 \times 10^{-5}$  Gyr, and the tolerance parameter  $\theta = 0.6$ . In order to obtain a starting position and velocity for the dwarf galaxy model, we refined iteratively an initial guess of these values, and required that the resulting orbit fit the velocity and position information of the Y03 SDSS and the 2MASS fields presented above, as well as the globular clusters. Acceptable orbits could be fit for both a co-rotating and a counter-rotating object, so we examine both cases below. These fitted orbits have an azimuthal period of 0.45 Gyr and 0.3 Gyr, respectively, for the co-rotating and counter-rotating models.

The initial dwarf galaxy was modeled with a King model with  $10^5$  particles. We experimented with several such models, trying out masses in the range of  $2 \times 10^8$  to  $10^9 M_{\odot}$  (the range suggested by Ibata et al. 2003, and which is consistent with the mass estimate derived above), and with different tidal radii and concentration parameters. Some fine-tuning of these parameters is needed to give both a stream and remnant that approximates the observed distribution. One of the better fitting models had a mass  $5 \times 10^8 M_{\odot}$ , tidal radius 2.5 kpc and  $W_0 = 4.5$ , and it is this model that we will discuss below. However, these values are by no means the required initial parameters of the satellite galaxy. They are sensitive to the orbit, and must therefore also be sensitive to the decay rate of the satellite due to dynamical friction, which we have neglected. The model is therefore only illustrative.

In the top panels of Figures 14 and 15, we show respectively the  $x$ - $y$  configuration (looking down onto the Milky Way from the north Galactic pole) at the end of the simulation, for the co-rotating and counter-rotating models. Given the simplicity of the assumptions the similarity between the simulations and observations is remarkable, though we feel that a formal statistical comparison is not very meaningful at this stage due to the fact that we have left out the self-gravity of the Milky Way. However, what the simulations do show is that the streams that arise naturally during the tidal disruption of a dwarf galaxy can be pulled out to be seen as multiple streams, even in the relatively short time ( $\sim 2$  Gyr) that we simulated. This may account for the different peaks in the distance modulus distribu-

tions (Figures 2 and 8). Figures 14 and 15 also show the positions of the globular clusters that have Galactocentric distances  $R_{GC} > 8$  kpc, and that lie within 8 kpc of the Galactic plane. To select the closest star clusters to our simulation, we choose somewhat arbitrarily a simple statistic:  $\chi^2 = \left(\frac{|\bar{x} - \bar{x}_{model}|}{2 \text{ kpc}}\right)^2 + \left(\frac{v_{\odot} - v_{\odot model}}{20 \text{ km s}^{-1}}\right)^2$ ; we list the globular and open clusters that have  $\chi < 3$  in the prograde and retrograde models, in Tables 1 and 2 respectively. We defer analyzing the likelihood of the alignment of these star clusters with the Canis Major stream to a future contribution when we present a more realistic simulation with a live Milky Way.

The distribution of the simulation particles projected onto the sky is shown in Figure 16; the models nicely reproduce the curving behaviour of the Northern Arc observed towards the Galactic anticentre (compare to Figure 4), the Canis Major over-density as well as the over-densities “A” and “B” (see Figure 5) seen towards  $\ell = 70^\circ$  and  $\ell = 300^\circ$ . The Heliocentric radial velocity profiles of the models are given in Figure 17. To our surprise, we find that current data do not appear to prefer the prograde model over the retrograde. Future measurements of the radial velocity of the stream in directions sufficiently far away from the Galactic anticentre should resolve this uncertainty.

The numerical simulations presented here lend support to the notion that the Canis Major over-density is the remnant of a larger accreted galaxy whose tidal disruption gave rise to the asymmetries in the Galactic M-giant distributions that we report above. If we accept this model, we find that the progenitor had an orbit that was closely aligned with the Galactic Plane (the orbit is inclined at only  $\sim 10^\circ$  from the Plane). It is unclear at present whether the object follows a prograde or a retrograde orbit, though a-priori the prograde case would appear to be more likely since it would allow for stronger interactions with the Galactic disk, due to which the orbit would have decayed to its present, rather circular, state. The remaining debris has an apocentre of  $\sim 20$  kpc and a pericentre close to the Solar radius. Indeed, according to the simulations displayed in Figures 14 and 15, the debris from the Canis Major dwarf streams through the Solar Neighbourhood. Comparing the kinematics of the Canis Major stream to the stream discovered by Helmi et al. (1999), the only other large stream known to pass close to the Sun, shows that the streams of our models have very different angular momentum. The angular momentum distribution of the particles within 2 kpc of the Solar Neighbourhood is shown in Figure 18; these particles display very different kinematics, and are unlikely to be associated to the Helmi et al. (1999) stream.

## 6 DISCUSSION AND CONCLUSIONS

We have shown that the distribution of M-giant stars at low latitude is highly asymmetric. The most striking over-density is due to an elliptical object present in the disk, in the direction of the Canis Major constellation in the southern Galactic hemisphere at  $D_{GC} = 12.0 \pm 1.2$  kpc. This structure contains as many M-giant stars as the remnant of the Sagittarius dwarf galaxy. A less dense structure, but of huge proportions, the Northern Arc curves around the Galaxy in the direction of the Galactic anticentre. This arc

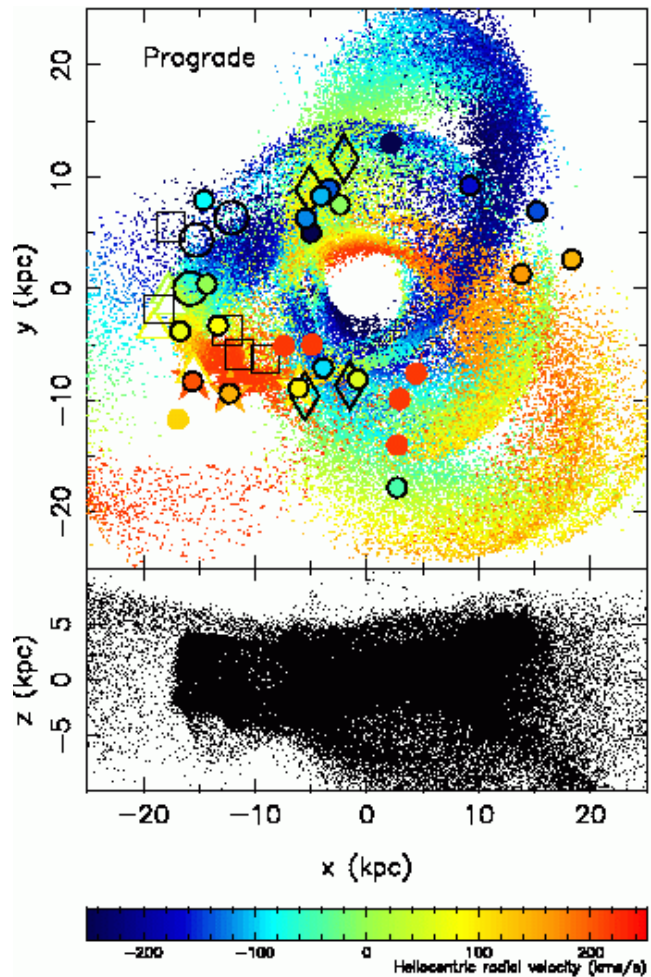


**Figure 14.** Two different projections of an N-body simulation of the disruption of the progenitor of the Galactic “Ring” and the Canis Major structure. The Galactic Centre is at the origin, and the Sun at  $(x, y, z) = -8, 0, 0$  kpc. The dwarf galaxy model was placed on an orbit that co-rotates with the Galactic disk. The upper panel shows the  $x$ - $y$  distribution (i.e. as seen from the Galactic north pole), with colour-coded radial velocities. In black, we show the positions and distances of the INT fields from Ibata et al. (2003) (large open circles), and the 2MASS data presented in this contribution (open squares and diamonds). The diamonds represent those fields for which a distance estimate was secured by summing in Galactocentric, rather than Heliocentric distance. The colour-coded graph markers show the positions, distances and velocities of the four SDSS fields from Yanny et al. (2003) (open triangles), and of the 4 globular clusters detailed in section 4 (star symbols). The filled circles represent all globular and open clusters of known radial velocity within 8 kpc of the Galactic plane, and that have Galactocentric distances  $R_{GC} > 8$  kpc; the subset of these that are circled black are those objects listed in Table 1, which are close in phase-space to the simulation particles. This velocity-distance-position coincidence with the model suggests that several globular clusters around the Milky Way may be associated with the Canis Major accretion event.

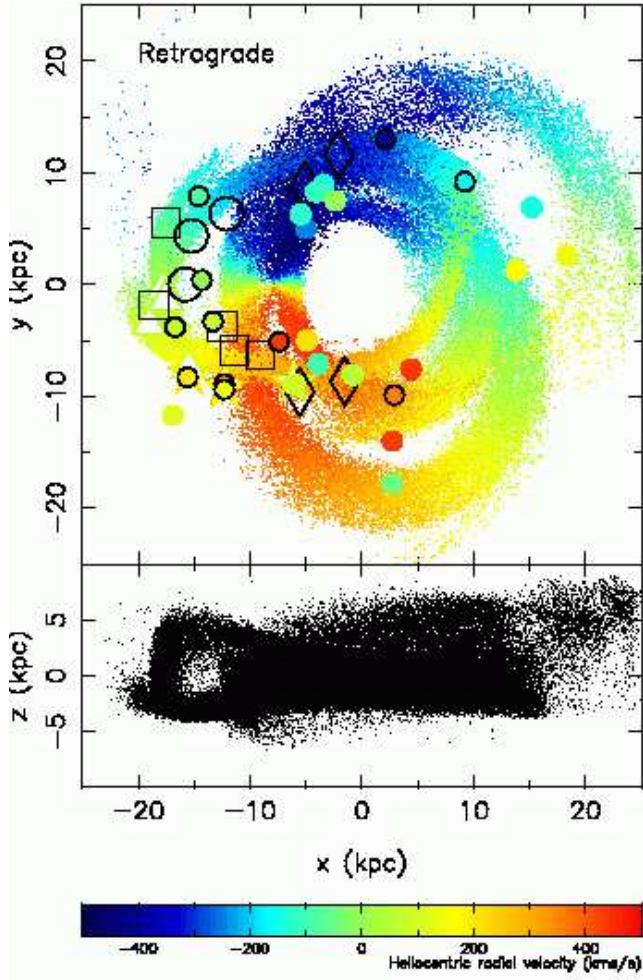


Figure 15. As Figure 14, but for a model on a retrograde orbit.

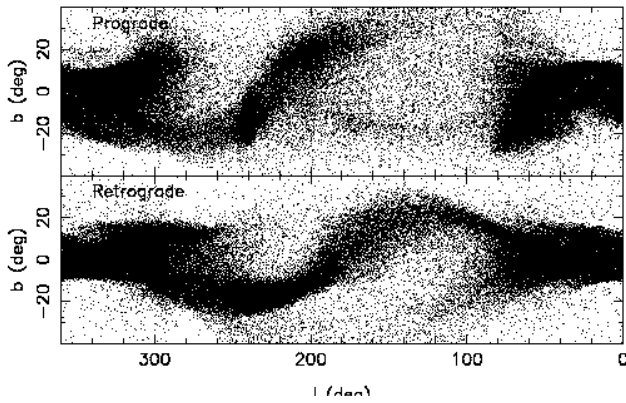


Figure 16. The  $l$ - $b$  distribution of the prograde model (upper panel) and retrograde model (lower panel). Most of the observed large-scale asymmetries of the Galactic M-giant distribution are reproduced in this projection of the simulations: the broad curved distribution of the Northern Arc seen towards the anticentre, the strong over-density seen towards Canis Major at  $l \sim 240^\circ$ ,  $b \sim -10^\circ$ , a weak feature similar to the “Southern Arc” is also present, plus the over-densities “A” and “B” at  $\Phi \sim 100^\circ$ , and  $\Phi \sim 260^\circ$ .

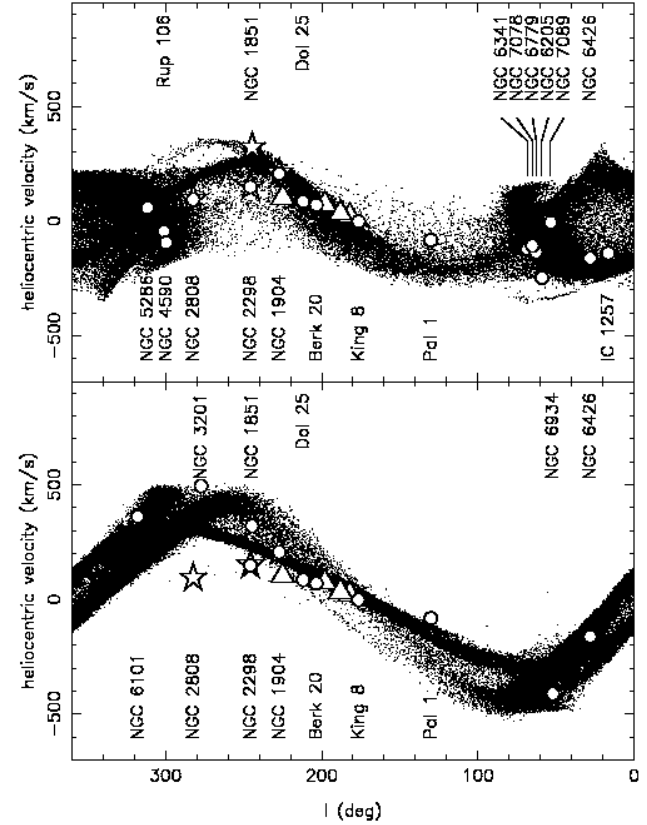


Figure 17. The Heliocentric radial velocity of the prograde model (upper panel) and retrograde model (lower panel) as a function of Galactic longitude, is compared to the Y03 SDSS fields (open triangles) and the 4 globular clusters NGC 1851, NGC 1904, NGC 2298, and NGC 2808 (star symbols). In addition, the open circles show, from right to left, the positions of the star clusters in Table 1 (for the top panel) and Table 2 (for the bottom panel), in the order listed.

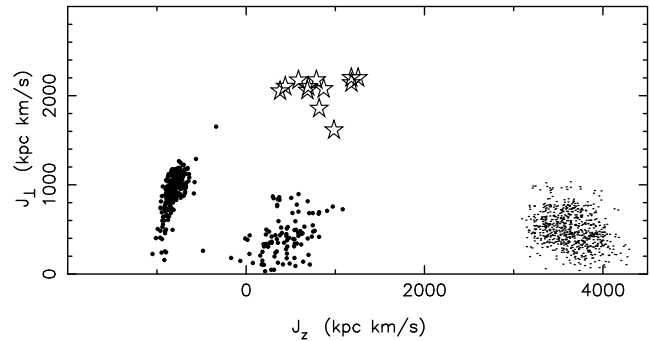


Figure 18. The larger dots show the angular momentum distribution of particles in the prograde simulation within 2kpc of the Sun, while the smaller dots show the same parameters for particles in the retrograde simulation. These distributions differ substantially from that found by Helmi et al. (1999) for the star stream detected in the Solar Neighbourhood (star symbols). The particles in both the Canis Major simulations follow a more planar orbit, with the prograde particles having typical Galactic disk kinematics. This large difference implies that the Canis Major stream is not associated with the Helmi et al. (1999) structure.

ranges from the Galactic plane at  $\ell \sim 230^\circ$  to  $b \sim +30^\circ$  at  $\ell \sim 140^\circ$ . Between  $140^\circ < \ell < 180^\circ$  it has a mean displacement of  $\sim 20^\circ$  above the Galactic Plane, with a distance of  $D_{GC} = 18.1 \pm 0.1$  kpc, it is separated from the disk in the radial direction along the line of sight, and has a Gaussian profile of width  $11.6^\circ \pm 1.9^\circ$ .

Several other structures are also detected. In the southern hemisphere, the ‘‘Southern Arc’’ population with Galactocentric distance  $12.0 \text{ kpc} < D_{GC} < 15.1 \text{ kpc}$  is observed between  $110^\circ < \ell < 210^\circ$ ; this may be the continuation of the southern hemisphere structure reported by Y03 for  $R_{GC} = 20 \pm 2$  kpc and  $180^\circ < \ell < 227^\circ$ . Two other over-densities are detected towards the Galactic bulge, and close to the Galactic Plane: one is found between  $230^\circ < \Phi < 270^\circ$  at  $D_{GC} < 14.5$  kpc, while the other is between  $90^\circ < \Phi < 130^\circ$  at  $D_{GC} = 10.5$  kpc.

Given these observations, we examine the idea of an in-plane accretion of a dwarf satellite galaxy onto the Milky Way. The realization that the four globular clusters NGC 1851, NGC 1904, NGC 2298, and NGC 2808, are close to each other in phase space and are also close in position and distance to the Canis Major over-density also lends strong support to this possibility. In this scenario the remnant of the satellite is likely the object in the direction of Canis Major. During the tidal disruption process, the dwarf galaxy loses stars in a long stream which loops around the Milky Way and is now seen as the Monoceros ‘‘Ring’’ structure. The two other hypotheses presented by I03 do not seem to be allowed by our observations. Indeed, the height of the structure (generally more than 3 kpc) could hardly be explained by a spiral arm. Furthermore, the multiple peaks in the distance distribution are more suggestive of multiple crossings of a stream rather than of a ring-like Galactic structure, produced by the dynamical evolution of ancient stellar warps.

The simple N-body models we presented reproduce many of the observed spatial features, including the Canis Major over-density, the vast ring-like arc towards the Galactic anticentre, the over-densities towards  $\ell = 70^\circ$  and  $\ell = 290^\circ$ , as well as faint debris scattered out to large distance below the Galactic Plane in the anticentre direction. The models also reproduce the available kinematic data and point to the possibility that several star clusters, apart from those close to the Canis Major over-density, could be related to the Canis Major Stream. The success of this simple model strongly suggests that many, if not all, of the asymmetries in the Galactic M-giant population presented above, are due to a single accretion event. The accreted satellite must have had an orbital plane closely aligned to the plane of the Milky Way galaxy. Our analysis shows that the ‘‘shell’’ model of Helmi et al. (2003) gives poor agreement with the observations, but we confirm the tidal stream model for the ‘‘Monoceros Ring’’ proposed by Y03.

The observations and model also suggest a connection to the Galactic thick disk. The orbital eccentricity of the model is  $e = (r_{apo} - r_{peri}) / (r_{apo} + r_{peri}) \sim 0.5$ , a value that is typical for Galactic thick disk stars of metallicity  $[\text{Fe}/\text{H}] \sim -1.2$  (Chiba & Beers 2000). Furthermore, the vertical exponential scale height of the debris  $0.73 \pm 0.05$  kpc, is very close to the thick disk value of 0.8 kpc determined by Reylé & Robin (2001). It is therefore possible that we have uncovered one of the galactic building blocks from which the

thick disk grows. This analysis suggests that the thick disk is continually growing, even up to the present time, through accretions of dwarf galaxies in co-planar orbits. Although with a progenitor mass of  $\sim 10^9 M_\odot$ , as suggested by our analysis, only a handful of accretions of the magnitude of that of the Canis Major dwarf galaxy are needed to populate the thick disk entirely. Globular clusters with disk-like kinematics may also have been brought to their present locations in this way. The observations and modeling we presented strongly support the analysis of Abadi et al. (2002), in which a large proportion of thick stars have their origin in accreted galaxy fragments. If the scenario we have developed here is correct, thick disks should be a generic component of giant spiral galaxies, since accretions are a generic feature of galaxy formation. Furthermore, at the edge of the disk where the dynamical times are longest, their structure will likely be a complex mess where streaming debris from the most recent accretions piles up at apocentre. These messy structures may indeed already have been detected in the Andromeda galaxy (Ibata et al. 2001b; Ferguson et al. 2002).

Further observational work is needed to constrain the kinematics of the structures we report here. These constraints are needed to determine whether the structure follows a prograde or a retrograde orbit, to verify the kinematic predictions of our models, as well as to guide future simulations. Detailed abundance distributions will also be invaluable in order to study the chemical difference between an accreted population, such as that of the Canis Major galaxy, and that of the normal Galactic disk. Future simulations with a live Milky Way will provide a more realistic comparison to the observations. It will be interesting to investigate the reaction of the Galactic disk stars and in particular the reaction of the HI gas, to this sizable accretion, while the back-reaction onto the Canis Major dwarf galaxy will be essential in order to model its dynamical evolution accurately.

## ACKNOWLEDGMENTS

We are grateful to A. Bragaglia and L. Monaco for useful suggestions and discussion, and to A. Helmi for kindly providing the kinematics of the Solar Neighbourhood stream stars. MB acknowledges the financial support to this research by the Italian Ministero dell’Università e della Ricerca Scientifica (MURST) through the grant p. 2001028879, assigned to the project *Origin and Evolution of the Galactic Spheroid*.

This publication makes use of data products from the Two Micron All Sky Survey, which is a joint project of the University of Massachusetts and the Infrared Processing and Analysis Center/California Institute of Technology, funded by the National Aeronautics and Space Administration and the National Science Foundation.

## REFERENCES

- Abadi M., Navarro J., Steinmetz M. & Eke V. *astro-ph/0212282*
- Bedin, L.R., Piotto, G., Zoccali, M., Saviane, I., Cassisi, S., & Bono, G., 2000, *A&A*363, 159

**Table 1.** Star clusters close in phase-space to the prograde model.

Name	$\ell$ (deg)	$ \bar{x} - \bar{x}_{model} $ (kpc)	$v_{\odot}$ (km s <sup>-1</sup> )	$v_{\odot model}$ (km s <sup>-1</sup> )	$\chi$
IC 1257	16.5	2.7	-140.2	-138.8	1.8
NGC 6426	28.1	2.2	-162.0	-148.3	1.7
NGC 7089	53.4	1.5	-5.3	15.8	1.6
NGC 6205	59.0	2.7	-246.6	-235.7	2.2
NGC 6779	62.7	1.0	-135.7	-137.1	0.2
NGC 7078	65.0	2.2	-107.3	-97.3	1.5
NGC 6341	68.3	0.9	-122.2	-114.3	0.4
Pal 1	130.1	2.6	-82.8	-88.0	1.8
King 8	176.4	0.9	-2.0	-9.9	0.4
Berk 20	203.5	0.8	70.0	69.6	0.1
Dol 25	211.9	1.1	85.0	73.8	0.6
NGC 1904	227.2	2.8	206.0	195.3	2.2
NGC 2298	245.6	3.3	148.9	150.9	2.7
NGC 2808	282.2	1.4	93.6	91.2	0.5
NGC 4590	299.6	2.5	-94.3	-102.0	1.7
Rup 106	300.9	1.6	-44.0	-33.2	0.9
NGC 5286	311.6	2.7	57.4	63.4	1.9

Data extracted from Harris (1996) and Merrillioid (1995). Column 2 states the Galactic longitude of the cluster; column 3 lists  $|\bar{x} - \bar{x}_{model}|$ , the difference in position between the simulation and the cluster; columns 4 and 5 list, respectively, the Heliocentric radial velocity of the cluster and simulation; finally, in column 6, we give the value of the  $\chi$  closeness statistic.

**Table 2.** Star clusters close in phase-space to the retrograde model (data arranged as in Table 1).

Name	$\ell$ (deg)	$ \bar{x} - \bar{x}_{model} $ (kpc)	$v_{\odot}$ (km s <sup>-1</sup> )	$v_{\odot model}$ (km s <sup>-1</sup> )	$\chi$
NGC 6426	28.1	1.6	-162.0	-169.0	0.7
NGC 6934	52.1	3.2	-411.4	-411.2	2.5
Pal 1	130.1	1.1	-82.8	-92.8	0.5
King 8	176.4	1.8	-2.0	-9.3	0.9
Berk 20	203.5	0.6	70.0	71.4	0.1
Dol 25	211.9	1.9	85.0	87.8	0.9
NGC 1904	227.2	2.8	206.0	201.1	2.0
NGC 1851	244.5	1.6	320.5	340.4	1.7
NGC 2298	245.6	1.9	148.9	150.7	0.9
NGC 3201	277.2	1.2	494.0	482.5	0.7
NGC 6101	317.8	0.5	361.4	361.1	0.1

Bellazzini, M., Fusi Pecci, F., Ferraro, F.R., Galletti, S., Catelan, M., & Landsman, W.B., 2001, AJ122, 2569  
 Bellazzini M., Ferraro F. R. & Ibata R. 2003a, AJ 125, 188  
 Bellazzini M., Ibata R., Ferraro F. R. & Testa V. 2003b, A&A 405, 577  
 Bellazzini M., Ibata R., Ferraro F. R., 2003c, in Satellites and Tidal Tails, D. Martinez-delgado and F. Prada Eds., S. Francisco, ASP, ASP Conf. Series, in press *astro-ph/0304502*  
 Burton W. & Te Lintel Hekkert P., A&ASupp 65, 427  
 Chiba, M., Beers, T. 2000, AJ 119, 2843  
 Clementini, G., Gratton, R., Bragaglia, A., Carretta, E., Di Fabrizio, L., Maio, M. 2003, AJ 125, 1309  
 Dehnen, W. & Binney, J. 1998, MNRAS 294, 429

Dehnen, W. & Binney, J. 1998, MNRAS 298, 387  
 Dehnen, W. (2000), ApJ 536, 39L  
 Dehnen, W. (2002), J. Comput. Phys. 179, 27  
 Ferguson, A., Irwin, M., Ibata, R., Lewis, G., Tanvir, N. 2002, AJ 124, 1452  
 Gómez-Flechoso, M.-A., Fux, R., Martinet, L. 1999, A&A 347, 77  
 Harris, W.E., 1996, AJ112, 1487  
 Helmi, A., White, S., de Zeeuw, T., Zhao, H.-S. (1999), Nature 402, 53  
 Helmi, A., White, S. (2001), MNRAS 323, 529  
 Helmi A., Navarro J., Meza A, Steinmetz M. & Eke V. 2003, ApJ 592L, 25  
 Ibata, R., Wyse, R., Gilmore, G., Irwin, M. & Suntzeff, N. 1997, AJ 113, 634  
 Ibata, R., Lewis, G. 1998, ApJ 500, 575  
 Ibata R., Lewis G., Irwin M., Totten E. & Quinn T. 2001, ApJ 551, 294  
 Ibata, R., Irwin, M., Lewis, G., Ferguson, A., Tanvir, N. 2001, Nature 412, 49  
 Ibata R., Lewis G., Irwin M. & Cambrésy L. 2002, MNRAS 332, 921  
 Ibata R., Irwin M., Lewis G., Ferguson A. & Tanvir N. 2003, MNRAS 340, 21  
 Majewski S., Skrutskie M., Weinberg M. & Ostheimer J. 2003, *astro-ph/0304198*  
 Martin, N. (2003), DEA thesis, Université de Strasbourg  
 Merrillioid, J.-C. 1995, in "Information and On-Line Data in Astronomy", Eds D. Egret & M.A. Albrecht (Kluwer Academic Press, Dordrecht), p. 127-138 The database for galactic open clusters (BDA)  
 Newberg H., et al. 2002, ApJ 569, 245  
 Reylé, C., Robin, A. (2001), A&A 373, 886  
 Rocha-Pinto H., Majewski S., Skrutskie M. & Crane J. 2003, ApJ 594, 115L  
 Schlegel D., Finkbeiner D. & Davis M. 1998, ApJ 500, 525  
 White, S., Rees, M. 1978, MNRAS 183, 341  
 White, S., Frenk, C. 1991, ApJ 379, 52  
 Yanny B., et al. 2003, ApJ 588, 824